

AD-A263 192



OFFICE OF NAVAL RESEARCH

Grant No. _____

R&T Code N00014-92-C-0173

Technical Report #02

DTIC
ELECTE
APR 21 1993
S C D

1

ADSORPTION OF SULFATE ON METAL ELECTRODES

by

**Leslie A. Barnes
Michael R. Philpott
Bowen Liu**

Prepared for publication

in the

Electrochemical Society Proceedings '93

**IBM Research Division, Almaden Research Center,
650 Harry Road, San Jose, CA 95120-6099**

1993

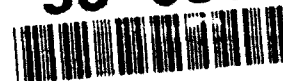
Reproduction in whole or in part is permitted
for any purpose of the United States Government

This document has been approved for public release
and sale; its distribution is unlimited

93 4 19 2 11

45732

93-08326



2278

REPORT DOCUMENTATION PAGE		READ INSTRUCTIONS BEFORE COMPLETING FORM.
1. REPORT NUMBER 02	2. GOVT ACCESSION NO	3. RECIPIENT'S CATALOG NUMBER
Technical Report 16 4. TITLE (and Subtitle) Adsorption of Sulfate on Metal Electrodes		5. TYPE OF REPORT & PERIOD COVERED Technical Report
		6. PERFORMING ORG. REPORT NUMBER
7. AUTHOR(s) Leslie A. Barnes Michael R. Philpott Bowen Liu		8. CONTRACT OR GRANT NUMBER(s) N00014-92-C-0173
9. PERFORMING ORGANIZATION NAME AND ADDRESS IBM Research Division, Almaden Research Center 650 Harry Road San Jose, CA 95120-6099		10. PROGRAM ELEMENT, PROJECT, TASK AREA & WORK UNIT NUMBERS
11. CONTROLLING OFFICE NAME AND ADDRESS Office of Naval Research 800 North Quincy Street Arlington, VA 22217		12. REPORT DATE 4/14/93
		13. NUMBER OF PAGES 19
14. MONITORING AGENCY NAME & ADDRESS (If different from Controlling Office) Dr. Ronald A. De Marco Office of Naval Research, Chemistry Division 800 N. Quincy Street Arlington, VA 22217 U.S.A.		15. SECURITY CLASS (of this report) Unclassified
		15a. DECLASSIFICATION/DOWNGRADING SCHEDULE
16. DISTRIBUTION STATEMENT (of this Report) Approved for public release; unlimited distribution.		
17. DISTRIBUTION STATEMENT (of the abstract entered in Block 20, if different from Report) Approved for public release; unlimited distribution.		
18. SUPPLEMENTARY NOTES Prepared for publication in Electrochemical Society Symposium Proceedings '93		
19. KEY WORDS (Continue on reverse side if necessary and identify by block number)		
20. ABSTRACT (Continue on reverse side if necessary and identify by block number) SEE NEXT PAGE		

The adsorption of sulfate (SO_4^{2-}) and bisulfate (HSO_4^-) on copper has been studied using *ab initio* calculations at the SCF level of theory, to aid in the interpretation of *in situ* experimental data from the electrochemical interface, in particular optical and surface X-ray measurements. The calculations are designed to give qualitative insight rather than quantitative accuracy. Optimized structures and harmonic frequencies and intensities are computed for isolated sulfate and bisulfate, and qualitative agreement with experimental data is demonstrated. The effect of a uniform electric field on sulfate is also studied. The structures of $\text{Cu}^0\text{SO}_4^{2-}$ and $\text{Cu}^0\text{HSO}_4^-$ are optimized. The bonding is dominantly ionic, with consequential small orientational dependence of the adsorbed ligand. We also compute structures for the larger $\text{Cu}_4^0\text{SO}_4^{2-}$ cluster. The sulfate ion is found to favour a "3-down" adsorption geometry with sulfate oxygens occupying on-top sites over the previously postulated "1-down" structure invoked to explain the early surface exafs experiments.

DTIC QUALITY INSPECTED 1

Accession For	
NTIS CRA&I	<input checked="" type="checkbox"/>
DTIC TAB	<input checked="" type="checkbox"/>
Unannounced	<input type="checkbox"/>
Justification	
By	
Distribution /	
Availability Codes	
Dist	Avail and/or Special
A-1	

Adsorption of Sulfate on Metal Electrodes

Leslie A. Barnes *, Michael R. Philpott and Bowen Liu
IBM Research Division, Almaden Research Center
650 Harry Road, San Jose, California 95120-6099

Abstract

The adsorption of sulfate (SO_4^{2-}) and bisulfate (HSO_4^-) on copper has been studied using *ab initio* calculations at the SCF level of theory, to aid in the interpretation of *in situ* experimental data from the electrochemical interface, in particular optical and surface X-ray measurements. The calculations are designed to give qualitative insight rather than quantitative accuracy. Optimized structures and harmonic frequencies and intensities are computed for isolated sulfate and bisulfate, and qualitative agreement with experimental data is demonstrated. The effect of a uniform electric field on sulfate is also studied. The structures of $\text{Cu}^0\text{SO}_4^{2-}$ and $\text{Cu}^0\text{HSO}_4^-$ are optimized. The bonding is dominantly ionic, with consequential small orientational dependence of the adsorbed ligand. We also compute structures for the larger $\text{Cu}_4^0\text{SO}_4^{2-}$ cluster. The sulfate ion is found to favour a "3-down" adsorption geometry with sulfate oxygens occupying on-top sites over the previously postulated "1-down" structure invoked to explain the early surface exafs experiments.

1 Introduction

Understanding the adsorption of sulfate on surfaces is a challenging scientific problem that is also of significant technological interest in connection with battery chemistry, dissolution of metals in acids, electroplating and polishing, and the incipience of oxide films. Recent optical and surface X-ray measurements of metal electrodes in contact with aqueous sulfate media have been explained with hypothetical models, with sulfate (SO_4^{2-}) and its hydrolysis product bisulfate (HSO_4^-) in specific orientations adsorbed on the metal surface [1]-[6]. Figure 1 shows some of these models.

The high symmetry (T_d) and many vibrational modes of sulfate that are exclusively IR or Raman allowed make it a potentially useful probe of forces influencing orientation and of the local field within the electrochemical double layer. Bisulfate, with lower symmetry, has more vibrational frequencies which may be IR or Raman allowed, some of which overlap with sulfate modes. This complicates interpretation

*Mailing Address: Mail Stop RTC-230-3, NASA Ames Research Center, Moffett Field, California 94035-1000

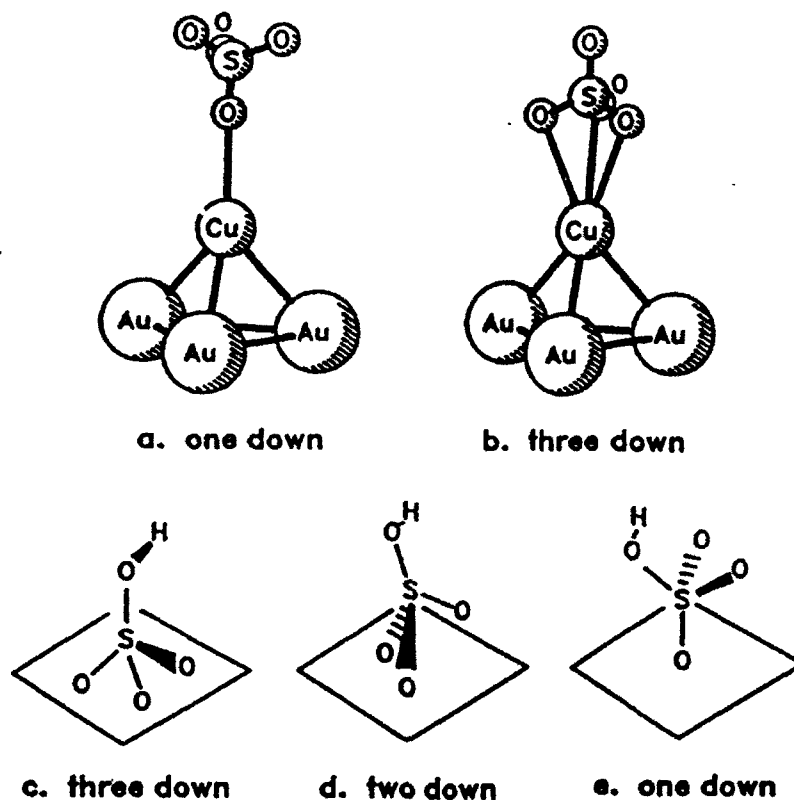


Figure 1: Proposed Sexafs model of sulfate on upd Cu monolayer on Au(111) surface along with some optical models for bisulfate.

of the experimental data, where both sulfate and bisulfate may be present. From a computational viewpoint, the larger size of sulfate and bisulfate make the calculation and interpretation of structures and spectra more difficult than for smaller ligands such as carbon monoxide or cyanide [7]. Nevertheless, because of the existence of several proposed structures on Cu surfaces [5, 6] and the variety of other data bearing on adsorption site geometry and structure [8]–[11], it is clear that model *ab initio* quantum chemical calculations could play a crucial role in elucidating geometry, structure and bonding at the adsorption site.

The goal of the present work is to use a series of simple models to explore the interaction of sulfate and bisulfate with metal surfaces and aid in the interpretation of *in situ* experiments. Previous calculations have studied Cu clusters with small ligands like O, CO, and CN^- [12]–[14]. On silver clusters the ligands F^- , Cl^- , Br^- , I^- , azide N_3^- , and thiocyanate SCN^- have been studied [15]–[18]. The polyatomic and potentially polydentate ligands SO_4^{2-} and HSO_4^- are more demanding of computational resources due to the larger number of atoms and electrons and the variety

performed [10]. Other structure determinations have used STM [30] and AFM [31] to obtain geometric information about the effect of sulfate on metal adatom sites on gold surfaces.

Optical spectroscopy has provided important information about adsorption of bisulfate and sulfate on metals and also how vibrational frequencies change on adsorption and with changes in electrode potential. In particular *in situ* surface FTIR spectroscopy [1]–[4], [32], has shown how sulfate, bisulfate and water adsorb on polycrystalline and single crystal surfaces and single crystals with submonolayer of under potentially deposited metals. Finally, we point out that other optical spectroscopies such as second harmonic generation and sum frequency generation [33] have provided some information concerning the interaction of adsorbed sulfate on metal electrodes over a wide range of potentials [34, 35].

3 Methods

For isolated SO_4^{2-} and HSO_4^- we carry out *ab initio* all-electron SCF calculations using analytical derivative methods to determine optimal geometries, harmonic frequencies, and both IR and Raman intensities. The SCF method is expected to give bond stretches which may be 10–20% too high compared to experiment. However, the results should be qualitatively correct. For SO_4^{2-} , we have also carried out geometry optimizations and frequency calculations in the presence of an applied electric field. These were carried out under the constraint that the S position was fixed. We have also computed IR intensities for SO_4^{2-} in the presence of an applied field, but not Raman intensities. For the single copper atom and copper cluster calculations with sulfate or bisulfate, we carry out *ab initio* all-electron SCF calculations using analytical derivative methods to determine optimal geometries, with the constraint of C_{3v} symmetry for $\text{Cu}^0\text{SO}_4^{2-}$ and C_s symmetry for $\text{Cu}^0\text{HSO}_4^-$. The $\text{Cu}_4^0\text{SO}_4^{2-}$ calculations were constrained so that the Cu_4 geometry was fixed at that of bulk Cu metal on the (111) surface [36] and the $\text{Cu}_4^0\text{SO}_4^{2-}$ cluster had C_{3v} symmetry.

The sulfur basis is derived from the (12s 7p) primitive Gaussian set of Dunning and Hay [37], contracted to [6s 4p] and supplemented with two *d* functions with exponent 0.9 and 0.3. The oxygen basis is the (9s 5p) primitive Gaussian basis set of Huzinaga [38], contracted to [4s 2p] according to Dunning [39]. This is supplemented with a diffuse *p* function with exponent 0.059 [37] and a *d* function with exponent 0.72 [40]. The basis for hydrogen is the (4s) primitive Gaussian set of Huzinaga, contracted to [2s] according to Dunning and Hay, and supplemented with a single *p* function with exponent 1.0. For Cu we use the (14s 9p 5d) primitive Gaussian basis set of Wachters [41], contracted to [8s 4p 3d] using his contraction scheme 2. Two diffuse *p* functions, as recommended by Wachters, and the diffuse *d* function of Hay [42] are added, yielding a final basis set of the form (14s 11p 6d)/[8s 6p 4d]. This basis should be adequate to describe the dominantly electrostatic interaction between the Cu 4s electron and SO_4^{2-} or HSO_4^- units.

of potential binding modes. We first examine the isolated sulfate and bisulfate ions, and then look at the effect of a strong electric field on sulfate. We then model the binding to the surface first with a single Cu atom, and then progress to larger clusters with four metal atoms, looking at geometries and relative binding energies, using all electron *ab initio* SCF Hartree-Fock calculations and analytical derivative methods. A more complete description of additional calculations for sulfate and bisulfate including adsorption on ten atom Cu clusters will be reported elsewhere [19].

This paper is organized in the following way. In § 2 we provide a survey of the experimental data. In § 3 we discuss the theoretical methods used, and in § 4 we present our results and discussion, first presenting results for SO_4^{2-} and HSO_4^- , then $\text{Cu}^0\text{SO}_4^{2-}$, $\text{Cu}^0\text{HSO}_4^-$ and $\text{Cu}_4^0\text{SO}_4^{2-}$.

2 Survey of Experimental Data

In this section we briefly describe some of the more important experimental work that this paper impacts. There are three main areas: adsorption, structure, and optical spectroscopy.

In aqueous solution sulfate belongs to the class of anion known to undergo specific adsorption [20, 21] in the range of electrode potential corresponding to a thermodynamically stable electrochemical double layer. In this process more weakly bound water molecules between the electrode and the ion are displaced and the ion makes physical contact with the surface atoms of the metal. This is the origin of the term "contact adsorption". Early discussions of this phenomena also considered whether a chemical bond was formed, but conventional wisdom now describes the adsorption as primarily physisorption. In practice contact adsorption results from a balance of opposing free energy interactions of the following type: electrostatics, enthalpies of hydration of ion and surface atoms, and entropy of displaced water molecules. Generally speaking, large ions (eg. I^- , Cs^+) contact adsorb whereas small ions (eg. F^- , Ca^+) do not. The contact adsorption series for noble and coinage metal electrodes immersed in aqueous electrolyte is $\text{BF}_4^- < \text{PF}_6^- < \text{ClO}_4^- < \text{F}^- < \text{HSO}_4^- < \text{SO}_4^{2-} < \text{Cl}^- < \text{SCN}^- < \text{Br}^- < \text{I}^-$ [21, 22]. Verification of contact adsorption for sulfate and bisulfate on metals has been demonstrated by a variety of classical electrochemical techniques including cyclic voltammetry [23]–[25], differential capacitance [26], and radio tracer analysis [27]–[29].

Structure determinations by surface X-ray scattering have proved very important because actual geometric information has been derived. For example Blum *et al.* [5, 6] proposed the first structure for sulfate adsorption. These results are particularly important because it was proposed that sulfate may occupy an on-top site with the Cu-O-S bond parallel to the normal of the (111) surface plane. Complimentary X-ray studies have been reported for various Au surfaces [8, 9]. Similar on-top site geometries have been proposed for adsorption on Cu(100), obtained by emersing the electrode from acidic sulfate solution prior to transfer into UHV where LEED was

S-01 2.80

S-01	2.70
S-02	3.06
S-03	2.72
\angle O3-S-O3	113.3°

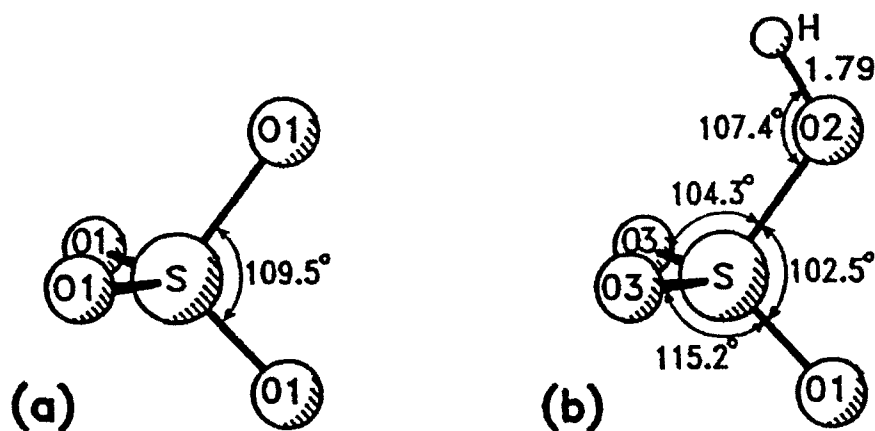


Figure 2: Isolated SO_4^{2-} and HSO_4^- structures. Bond lengths are in a.u. and angles are in degrees (1 a.u. = 0.529177 Å).

The programs CADPAC [43] and the Cambridge Direct SCF [44] are used, implemented on an IBM 3090/300J and RISC SYSTEM/6000 computers at the IBM Almaden Research Center. CADPAC was modified to compute frequencies and intensities in the presence of an applied electric field according to the methods of Duran *et al.* [45].

4 Results and Discussion

4.1 Isolated SO_4^{2-} and HSO_4^- ions

To illustrate the qualitative accuracy of the calculations, we consider here the structure and vibrational frequencies of isolated SO_4^{2-} and HSO_4^- . We emphasize, however, that our results are for "gas-phase" species — so the comparison with experiment will only be qualitative. Nevertheless, the results are useful.

The structure of isolated SO_4^{2-} and HSO_4^- are illustrated in Figure 2. Isolated SO_4^{2-} has tetrahedral symmetry (T_d point group), whereas HSO_4^- has a single plane of symmetry (C_s point group). The computed bond distance for SO_4^{2-} of 2.80 a.u. is in good agreement with the experimental value of 2.82 a.u., which is the value in the Na_2SO_4 crystal and also is the average value in the K_2SO_4 crystal [36]. The computed

Table 1: Summary of the SO_4^{2-} harmonic frequencies and intensities

Mode	Freq. cm^{-1}	IR int. km/mol	Raman int. $\text{\AA}^4/\text{amu}$	Expt. Freq. ^a cm^{-1}
$\nu_2(e)$	471	0	2.3	451
$\nu_4(t_2)$	666	50	2.4	618
$\nu_1(a_1)$	1035	0	24.6	981
$\nu_3(t_2)$	1174	605	8.2	1104

^a Aqueous Na_2SO_4 [49]

structure of HSO_4^- is also in general agreement with data from crystal structures of KHSO_4 [46] and NH_4HSO_4 [47]. For example, in KHSO_4 the S–O3 distance is around 2.72 a.u., whereas the S–O1 distance is longer at around 2.77 a.u., due to hydrogen bonding with other HSO_4^- units in the crystal. The S–O2 distance is around 2.96 a.u. in the crystal, shorter than the theoretical result, again an effect due to hydrogen bonding in the crystal. The O–H distance is only 1.37 a.u. in KHSO_4 and NH_4HSO_4 , compared with the 1.79 a.u. value found here. This difference is larger than could reasonably be expected. However, as discussed by Nelmes [47], the “expected” O–H bond distance in other hydrogen bonded systems is in the range 1.8–1.9 a.u. For example, the O–H distance in H_2SO_4 [2, 48] is 1.83 a.u. Therefore the theoretical value seems very reasonable. Regarding the angles, there is again qualitative agreement, except for the $\angle\text{S–O–H}$ which is not unexpected based on the bond distance differences. For example, in KHSO_4 , the $\angle\text{O3–S–O2}$ is around 105° , compared with 104° theoretically, and the $\angle\text{O3–S–O1}$ is 111° compared with 115° theoretically. There is some difficulty making direct comparisons, due to hydrogen bonding and other “crystal” effects — however, the theoretical results are qualitatively correct. Thus, for HSO_4^- , the lengthening of the S–OH bond distance and the shortening of the other S–O distances compared with the S–O distance in SO_4^{2-} is seen in both the experimental and theoretical results, and the changes in the bond angles are also in the same general direction.

The computed frequencies and intensities for SO_4^{2-} are given in Table 1 and are in good agreement with the aqueous Na_2SO_4 results, although the symmetric stretch is too high, as expected at the SCF level of theory. In general, frequencies which are too high also correlate with bond distances which are too short at the SCF level of theory — however, external media effects in the solution or crystal environment make specific comparison between the frequencies and bond lengths difficult. In fact the agreement between the computed and experimental frequencies is somewhat fortuitous — the aqueous results will undoubtedly be affected by factors such as hydrogen bonding [49], whereas the effect of electron correlation has not been

Table 2: Comparison of computed HSO_4^- frequencies and intensities with experiment

	Freq. cm^{-1}	IR int. km/mol	Raman int. $\text{\AA}^4/\text{amu}$	Expt. Freq. ^a cm^{-1}
a''	130	93	2.3	145
a'	441	4	1.5	447
a''	476	11	1.1	418 ^b
a'	616	52	2.8	576
a''	641	71	2.8	589
a'	642	27	3.8	610
a'	861	330	9.5	883
a'	1157	123	18.4	1022
a'	1258	132	3.0	1044
a''	1351	521	4.7	1194
a'	1409	467	4.0	— ^c
a'	4176	73	61.2	3510

^a Frequencies from Raman spectrum of NH_4HSO_4 crystal (See reference [49] and references therein)

^b There is another a'' mode reported at 407 cm^{-1}

^c Frequencies in the range $1360\text{--}1390 \text{ cm}^{-1}$ have been reported from IR spectra of molten KHSO_4 (See reference [49] and references therein)

accounted for in the calculations. However, the qualitative agreement is good, the pattern of vibrational levels being well reproduced. For the intensities there are no absolute measurements. However, it is known that ν_3 is the most intense IR band for SO_4^{2-} , and that ν_1 is the most intense Raman band, which is clearly demonstrated in the theoretical results.

The computed harmonic frequencies and intensities of HSO_4^- are given in Table 2. We denote them according to their symmetry label in the C_s point group. We also present experimental frequencies for HSO_4^- in the NH_4HSO_4 crystal, taken from the work of Dawson *et al.* [49]. We see overall qualitative agreement between the theoretical and experimental frequencies, with the S-O stretches being somewhat too high as found for SO_4^{2-} , except for the S-OH stretch which is too low, possibly correlating with the error found for the S-OH bond distance, which was too long. Quantitative agreement should not be expected due to both limitations in the theory and other effects such as additional hydrogen bonding in the solid, which is expected to lower the experimental O-H stretching frequency. As far as the intensities are concerned, the computed results seem to be in fair agreement with the experimentally observed values in that the most intense Raman band experimentally is the $1022\text{--}1044 \text{ cm}^{-1}$ band and this corresponds to the 1157 cm^{-1} band in the theoretical calculations.

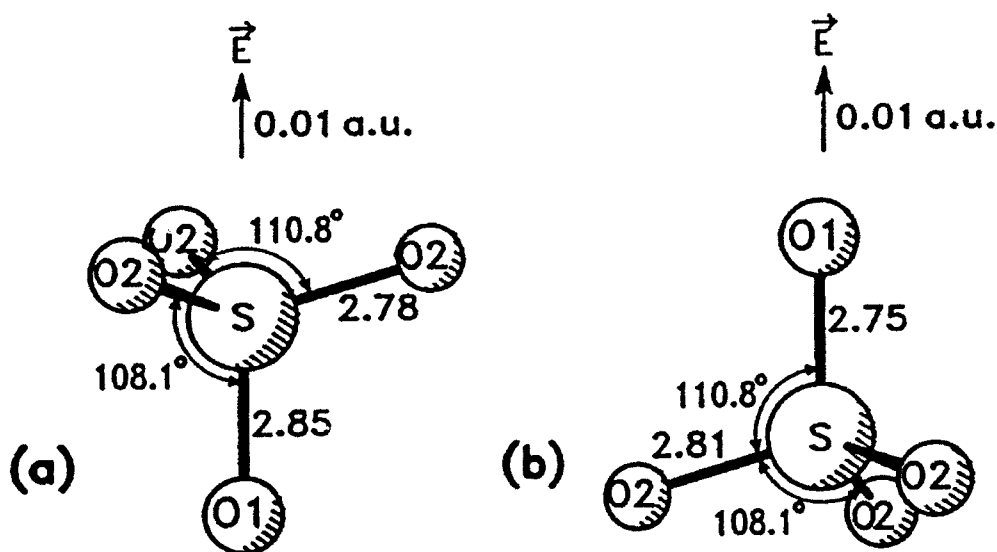


Figure 3: SO_4^{2-} structure in the presence of an electric field along a C_3 axis. Bond lengths are in a.u. and angles are in degrees (for the electric field, 1 a.u. = 5.14221×10^9 V/cm).

Furthermore the order and relative intensity of the four bands at 642, 862, 1157, and 1258 cm^{-1} are not expected to change because all these modes have the same symmetry. Overall, the theoretical methods used here give useful qualitative, though not quantitative, results.

4.2 SO_4^{2-} in the presence of an electric field

In this section we consider the effect of an applied electric field on the structure, frequencies and IR intensities of SO_4^{2-} . This analysis is useful as a simple model of electric field effects at an electrode surface, and also in the analysis of binding in the copper plus sulfate clusters. The magnitude of the field was fixed at 0.01 a.u. (5×10^7 V/cm), corresponding to the strong electric field expected in the electrochemical double layer [13, 50].

The effect of the applied field on the structure of SO_4^{2-} is illustrated in Figure 3. The field is applied along a C_3 axis, with a positive and negative sign, and the SO_4^{2-} unit has C_{3v} symmetry in both cases, with different bond distances and angles. Considering first Figure 3(a), we see that the S-O1 bond has lengthened significantly from the isolated ion value of 2.80 a.u., whereas the S-O2 bond has shortened. However, the shortening effect is smaller since the S-O2 bond lies at a greater angle to the applied field. The bond angles show effects consistent with the distances. The O1-S-O2 angle has *decreased* from the isolated ion value of 109.5° , whereas the O2-S-O2 angle has *increased*. Thinking of the S position as fixed, we see that all the O atoms have

Table 3: Summary of the SO_4^{2-} frequencies (cm^{-1}) and IR intensities (km/mol) with an electric field along S-O1 (C_{3v} symmetry)

	-0.01 ^a a.u.		+0.01 ^b a.u.	
	ν	IR int.	ν	IR int.
$\nu_2(e)$	471	0.1	471	0.1
$\nu_4(e)$	666	54.2	665	44.6
$\nu_4(a_1)$	664	37.8	667	58.8
$\nu_1(a_1)$	1015	138.2	1028	20.3
$\nu_3(e)$	1210	583.0	1136	626.3
$\nu_3(a_1)$	1113	517.3	1248	547.5

^a The orientation of the field corresponds to Figure 3(a)

^b The orientation of the field corresponds to Figure 3(b)

moved in the direction opposite to the applied field, as may be expected due to their negative charge. Reversing the direction of the applied field (Figure 3(b)) has the expected effect — the O atoms all move in the opposite direction, so that the bond distances and angles change in the opposite sense but by about the same magnitude as for the first field direction.

The computed harmonic frequencies and IR intensities for SO_4^{2-} in the presence of an applied electric field are given in Table 3, which are to be compared with the isolated ion results of Table 1. The frequencies in Table 3 are identified by the original labels ($\nu_1 - \nu_4$) used in Table 1, as the assignment is quite clear even though the symmetry is lower. We see that the t_2 modes of the T_d point group have split into a_1 and e modes for the C_{3v} point group in the presence of the applied field. Also, ν_2 and ν_4 are barely affected by the applied field, presumably because these modes involve motions which are predominantly perpendicular to the applied field. Because of their low IR and Raman intensity, these modes are difficult to detect experimentally.

Of more interest are ν_1 and ν_3 , as these are intense in the Raman and IR regions, respectively (see Table 1). Although we have not computed Raman intensities in the presence of an applied field, it is likely that ν_1 will still be the most intense Raman band in this case also. From Table 3, for the -0.01 a.u. field, we see that the lengthening of the S-O1 bond (Figure 3(a)) results in a reduction of the $\nu_1(a_1)$ mode by about 20 cm^{-1} and the $\nu_3(a_1)$ mode by about 60 cm^{-1} , a large effect. In addition, ν_1 has gained some IR intensity, possibly due to interaction with the intense $\nu_3(a_1)$ mode. The $\nu_3(e)$ mode has increased in frequency by about 35 cm^{-1} , reflecting the shorter S-O2 bond distance. We note that ν_1 involves both S-O1 and S-O2 stretches, so that in the presence of the applied field there is a balance between effects which increase ν_1 (shortening the three S-O2 distances) and decrease ν_1 (lengthening the

S-O1 distance).

From the +0.01 a.u. results of Table 3, we see that reversing the direction of the applied field has a similar effect on the frequencies as for the bond distances. The $\nu_1(a_1)$ mode is again reduced in frequency, although the effect is smaller than for the -0.01 a.u. field. This shows, however, that an intuitive guess based on the bond distances is not entirely appropriate for predicting the frequency shifts — in this case, the additional $\nu_3(a_1)$ mode has an effect on the $\nu_1(a_1)$ mode, in one case moving down in frequency and the other case moving up. It is probable that this shift in $\nu_3(a_1)$ has a subtle but important effect on $\nu_1(a_1)$ for the -0.01 a.u. field case, increasing the IR intensity and reducing the frequency. Further evidence for this may be seen from the IR intensity of $\nu_1(a_1)$ in the +0.01 a.u. field case — the increase is much smaller than for the -0.01 a.u. case, because $\nu_3(a_1)$ has moved up in frequency rather than down. The $\nu_3(e)$ modes are shifted down in frequency for the +0.01 a.u. field case, as expected.

If we were to consider the metal surface to be perpendicular to the applied field direction, then we must keep in mind the fact that the e modes will not be observable on a surface. This is because the IR intensity arises from a dipole moment derivative which is parallel to the "surface", which will be cancelled by image charge effects (ie. the surface selection rule). Therefore it is the a_1 modes which are the most important, as these involve dipole moment derivatives which are perpendicular to the "surface". These simple model calculations indicate that the orientation of the SO_4^{2-} molecule on the surface may be determined by the frequency shift of the intense $\nu_3(a_1)$ mode.

4.3 $\text{Cu}^0\text{SO}_4^{2-}$ results

In this section we consider two $\text{Cu}^0\text{SO}_4^{2-}$ structures, illustrated in Figure 4, denoting them as "1-down" and "3-down", respectively. There are other structures which may be important — for example, there is a "1.5 down" structure with a Cu-O1-S angle of 122° . This lies around 2 kcal/mol below the 1-down structure. In the current work we consider only the C_{3v} structures, postponing discussion of alternative structures to future work [19]

The interaction of SO_4^{2-} with the Cu atom is mainly electrostatic, dominated by charge-induced dipole interactions. Remembering that SO_4^{2-} has no permanent dipole moment, this means that the binding energy of SO_4^{2-} to a single Cu atom is not especially sensitive to the orientation of the SO_4^{2-} unit. The $4s$ electron on Cu polarizes away from the SO_4^{2-} unit, forming an sp hybrid orbital in order to both reduce the repulsion and create an attractive electrostatic interaction by forming a positive region of charge on the SO_4^{2-} side of the atom — an induced dipole. The interaction is strong — the binding energy of the structure illustrated in Figure 4(a) is around 37 kcal/mol. For comparison, at an equivalent level of theory the binding energy of $\text{Cu}^0\text{H}_2\text{O}$ is less than 1 kcal/mol (a Van der Waals complex), whereas the binding energy of $\text{Cu}^+\text{H}_2\text{O}$ is strong at around 32 kcal/mol.

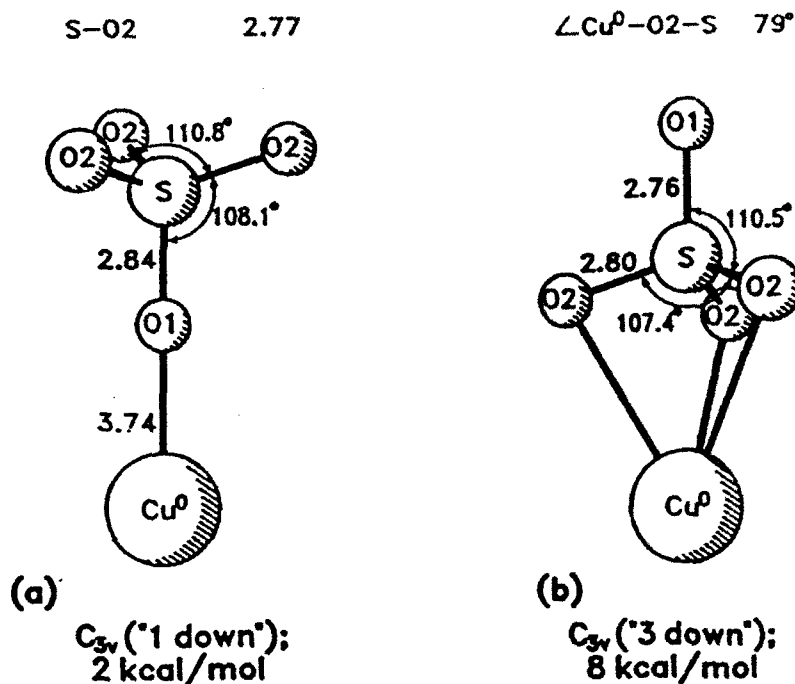


Figure 4: Summary of $\text{Cu}^0\text{SO}_4^{2-}$ structures in C_{3v} symmetry. Bond lengths are in a.u. and angles are in degrees.

The two structures are separated energetically by 6 kcal/mol. The Cu-O bond distances in each case are very different. The Cu-O1 distance of the 1-down structure is reasonable — for example, the early surface exafs experiments [5] found a value of 3.9 a.u. The Cu-O2 distance of 4.83 a.u. for the 3-down structure is much greater — in this case the limiting factor is the inability of the SO_4^{2-} unit to distort sufficiently to allow a stronger interaction between the O2 atoms and the Cu, combined with the repulsion between the formally positively charged S and the positive charge due to the induced dipole on the Cu atom. The fact that there are three O2 atoms involved in the interaction offsets these factors to some extent.

It is of interest to compare the bond lengths and angles of the SO_4^{2-} unit in $\text{Cu}^0\text{SO}_4^{2-}$ (Figure 4) with those of SO_4^{2-} in the presence of an applied field (Figure 3). For the 3-down structure, we note that the S-O2 distance is the same as in free SO_4^{2-} , in contrast to Figure 3(b), where it is slightly longer. However, the O2-S-O2 angle is smaller for the 3-down structure than in Figure 3(b). These differences are due to the more localized nature of the electrostatic interaction between Cu and SO_4^{2-} compared with the uniform electric field of Figure 3. Overall, however, there is a remarkable similarity between the SO_4^{2-} unit in the 1-down structure and the applied field structure of Figure 3(a), and the SO_4^{2-} unit in the 3-down structure and the applied field structure of Figure 3(b). This is due to the dominantly electrostatic nature of the interaction of SO_4^{2-} with Cu — the Cu atom with an induced dipole is quite similar to an applied electric field, as far as the SO_4^{2-} unit is concerned. In

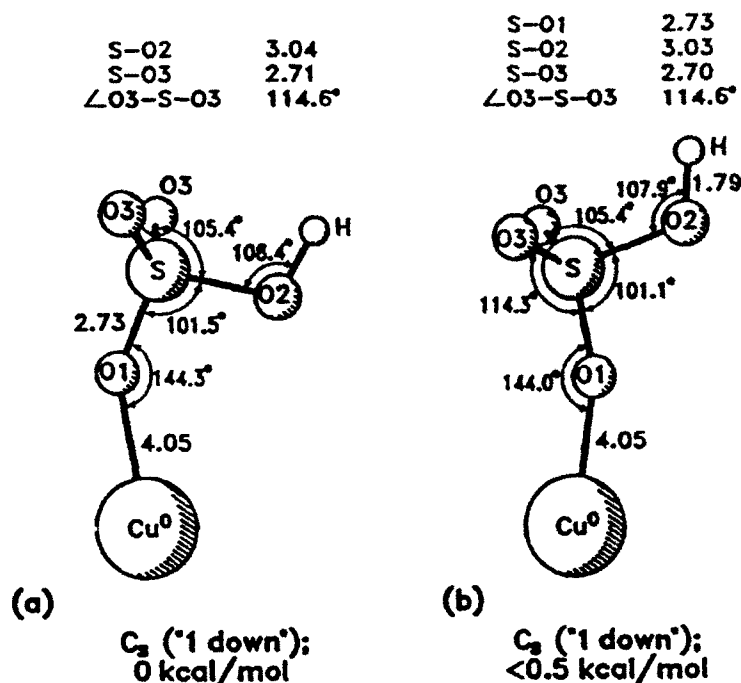


Figure 5: Summary of $\text{Cu}^0\text{HSO}_4^-$ structures in C_s symmetry. Bond lengths are in a.u. and angles are in degrees.

future work [19] we will consider whether this also applies to the frequency shifts for the SO_4^{2-} unit in $\text{Cu}^0\text{SO}_4^{2-}$. At the present time we simply state that they are expected to be qualitatively similar to those found for SO_4^{2-} in the presence of an applied field.

4.4 $\text{Cu}^0\text{HSO}_4^-$ structure

We now consider two $\text{Cu}^0\text{HSO}_4^-$ structures, illustrated in Figure 5. As for $\text{Cu}^0\text{SO}_4^{2-}$, there are other possible structures. However, these are the lowest energy structures which we have found.

There are two important differences between SO_4^{2-} and HSO_4^- , both due to the presence of the H in HSO_4^- . The first is the reduced charge of HSO_4^- , which results in a smaller charge-induced dipole interaction in $\text{Cu}^0\text{HSO}_4^-$. This is illustrated by the reduced binding energy of $\text{Cu}^0\text{HSO}_4^-$, only around 14 kcal/mol, less than half that of $\text{Cu}^0\text{SO}_4^{2-}$. The second difference is the presence of a permanent dipole moment in HSO_4^- . Considering Figure 2(b), the permanent dipole is oriented in the S-O2-H plane, approximately perpendicular to the O3-S-O3 plane, passing through the S with the positive end at the OH end of the molecule. There will be an effect which tends to orient the dipole to maximize the dipole-induced dipole interaction. However, this is a secondary effect compared with the charge-induced dipole interaction. This is illustrated by the two structures shown here — the orientation of the dipole is

different in each case, yet the structures have very similar energies.

The Cu-O1 bond distance is longer in $\text{Cu}^0\text{HSO}_4^-$ than $\text{Cu}^0\text{SO}_4^{2-}$, reflecting the lower binding energy of $\text{Cu}^0\text{HSO}_4^-$. Comparing the HSO_4^- structure in $\text{Cu}^0\text{HSO}_4^-$ with the isolated HSO_4^- structure of Figure 2(b), we see similar effects to the SO_4^{2-} structural changes in $\text{Cu}^0\text{SO}_4^{2-}$, but again these are not as large since the interaction is weaker. In addition, the symmetry is lower. The S-O1 bond distance is greater in $\text{Cu}^0\text{HSO}_4^-$ compared with HSO_4^- , and the S-O2 and S-O3 distances are shorter. The angles also change in a way consistent with that found for SO_4^{2-} in $\text{Cu}^0\text{SO}_4^{2-}$ — the negatively charged oxygens move toward the positive side of the Cu, whereas the positively charged H moves away. This decreases the O1-S-O2 angle, for example, and increases the S-O2-H angle.

There are several other possible structures for $\text{Cu}^0\text{HSO}_4^-$ when compared to $\text{Cu}^0\text{SO}_4^{2-}$, mainly because of the lower symmetry of HSO_4^- compared to SO_4^{2-} . However, the most important difference between $\text{Cu}^0\text{SO}_4^{2-}$ and $\text{Cu}^0\text{HSO}_4^-$, that is the weaker binding leading to smaller geometric distortions of HSO_4^- in $\text{Cu}^0\text{HSO}_4^-$, will also apply in these other cases. This also means that, if HSO_4^- and SO_4^{2-} adsorb on a Cu surface with a similar orientation, the frequency shifts for HSO_4^- may be expected to be smaller than for SO_4^{2-} . However, since the frequency shifts are very dependent on the orientation, this cannot be taken as a general rule.

4.5 $\text{Cu}_4^0\text{SO}_4^{2-}$ structures

In this section we present results for two structures of $\text{Cu}_4^0\text{SO}_4^{2-}$, illustrated in Figure 6. These are chosen to illustrate important limitations in the single copper atom model, but also to illustrate the utility of that model in the qualitative understanding of the interaction of SO_4^{2-} and a copper surface.

One valid question is why consider the single copper atom calculations at all, given that we are also presenting the Cu_4 results. There are several reasons — firstly, it is computationally feasible to compute harmonic frequencies and IR intensities for $\text{Cu}^0\text{SO}_4^{2-}$ and related systems. Although we have not presented these results here, this will appear in future work [19]. Secondly, the $\text{Cu}^0\text{SO}_4^{2-}$ results give good insight into the nature of the Cu- SO_4^{2-} interaction, without the additional complications of cluster artifacts which may appear (see below). Finally, the single copper calculations serve as a starting point from which to plan the more computationally intensive Cu_4 calculations.

The four atom copper cluster used here illustrates the additional binding possibilities of SO_4^{2-} on the Cu(111) surface — the 3-down and 1-down models now contain interactions with *three* copper atoms. Before discussing $\text{Cu}_4^0\text{SO}_4^{2-}$, however, we must note some additional limitations of the cluster model.

For the Cu_4 and the $\text{Cu}_4^0\text{SO}_4^{2-}$ clusters, we have currently used a closed-shell singlet coupling of the Cu 4s electrons. There are other possible couplings — in particular, several triplet states, which we will be studying in future work. Whether

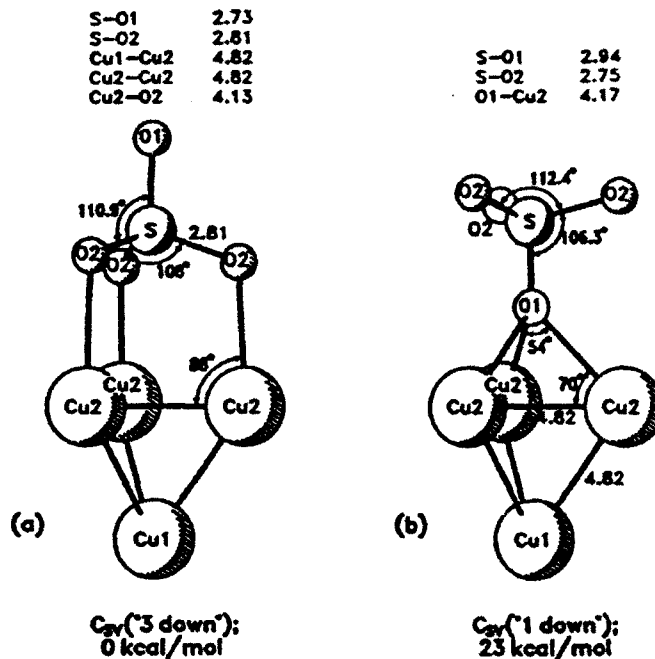


Figure 6: Summary of $\text{Cu}_4^0\text{SO}_4^{2-}$ structures showing ontop and three fold hollow sites. Bond lengths are in a.u. and angles are in degrees.

a singlet or triplet coupling of the electrons is chosen, there are problems which arise from using the cluster model. Cu_4 is in reality a small molecule with a valence shell of 4s-like electrons, rather than an accurate model of a metal surface. The occupation of the valence shell leads to an asymmetric charge distribution in C_{3v} symmetry, so that Cu1 in Figure 6 carries a net negative charge and the three Cu2 atoms carry an equal net positive charge, for the closed-shell singlet coupled case. This gives the cluster an overall dipole moment which in this orientation favours the binding of a negative ion such as SO_4^{2-} , and so absolute binding energies are not well defined. However, relative binding energies should still be qualitatively useful.

The two structures of Figure 6 illustrate the importance of multidentate bonding for SO_4^{2-} on copper. The 3-down structure is much more stable than the 1-down structure over the 3-fold hollow site. The binding energy of SO_4^{2-} to Cu_4 (closed shell singlet coupled) for the 3-down structure is 54 kcal/mol, compared with 31 kcal/mol for the 1-down structure. The binding energy for the 3-down structure is also much higher than that of SO_4^{2-} bound to Cu (37 kcal/mol, § 4.3). Some part of the increased binding energy for the Cu_4 cluster in the 3-down orientation is due to the permanent dipole moment of the Cu_4 cluster. However, the large difference of 23 kcal/mol between the 3-down and 1-down cases for $\text{Cu}_4^0\text{SO}_4^{2-}$ indicates that the 3-down structure may be favoured on Cu(111). Interestingly, the Cu-O distances are very similar for both cases, just over 4.1 a.u. However, the interaction of three negatively charged O atoms in the 3-down case obviously leads to a much stronger interaction than the

1-down case. The Cu-O bond length of 4.1 a.u. is reasonable when compared with the surface exafs value of 3.9 a.u. discussed previously. However, we do not expect quantitative agreement.

It is useful to compare the structures of the SO_4^{2-} units in Figure 6 with the earlier Figures 3 and 4. The SO_4^{2-} unit for the 3-down structure of Figure 6(a) is quite similar to that of Figure 3(b), indicating again a dominantly electrostatic interaction. Compared to the $\text{Cu}^0\text{SO}_4^{2-}$ result (Figure 4(b)), the angles of the SO_4^{2-} unit in the $\text{Cu}_4^0\text{SO}_4^{2-}$ 3-down structure indicate less distortion, due to the oxygens being in a more favourable position in the $\text{Cu}_4^0\text{SO}_4^{2-}$ structure. The 1-down $\text{Cu}_4^0\text{SO}_4^{2-}$ structure, although much higher in energy, is still interesting. We see again qualitative similarities to the earlier results of Figures 3(b) and 4(b). However, the distortions of the angles and the S-O1 bond distance are much greater in the 1-down $\text{Cu}_4^0\text{SO}_4^{2-}$ structure. Although the interaction is probably still dominantly electrostatic for the 1-down structure, the very long S-O1 bond distance may be indicative of the formation of a weak chemical bond between the Cu_4 cluster and the SO_4^{2-} unit. Comparing the bond lengths and angles of the $\text{Cu}_4^0\text{SO}_4^{2-}$ 1-down structure with those of HSO_4^- (Figure 2(b)), we see qualitative similarities. Although the distortions are not as large in $\text{Cu}_4^0\text{SO}_4^{2-}$ as in HSO_4^- it is clear that the 1-down structure is some way along to a chemically bonded species, in contrast to the 3-down structure, which is electrostatically bound.

Regarding frequency shifts for SO_4^{2-} in $\text{Cu}_4^0\text{SO}_4^{2-}$, we simply note from the geometric distortions of the SO_4^{2-} units that they are expected to be qualitatively similar to those found for SO_4^{2-} in the presence of an applied field, and the 1-down shifts may be larger than the 3-down shifts.

5 Conclusions

A series of model calculations have been presented which aim at helping to interpret the results of *in situ* experimental data on the adsorption of SO_4^{2-} and HSO_4^- on metal surfaces. The current calculations are aimed at adsorption on copper, but the qualitative nature of the results means that the conclusions may generalize to other metals. The geometry optimization, harmonic frequency and intensity calculations for isolated SO_4^{2-} and HSO_4^- indicate useful qualitative accuracy. The application of a strong uniform electric field to SO_4^{2-} gave insight into the response of SO_4^{2-} to the local field in the electrochemical double layer, and also gave insight into the nature of the bonding of SO_4^{2-} to Cu and Cu_4 . The frequency shifts computed for SO_4^{2-} in the presence of the applied field could be straightforwardly interpreted in terms of the geometrical distortions caused by the field. However, the calculations show that there are some subtle effects for the frequency shifts due to the interaction of modes of the same symmetry which are not obvious from intuitive arguments based on the geometrical distortions. In addition, the calculations show that the frequency shift of the most intense a_1 mode may serve to indicate the adsorption geometry of SO_4^{2-} on

Cu(111), assuming C_{3v} symmetry.

The interaction between Cu^0 and SO_4^{2-} or HSO_4^- is dominantly ionic, a charge-induced dipole interaction, so there is not a large energetic difference between the different structures. The binding energy of SO_4^{2-} to Cu or Cu_4 is quite high, whereas the binding energy HSO_4^- to Cu is lower due to the reduced charge of HSO_4^- , giving a reduced charge-induced dipole interaction. The similarity of the structure of the SO_4^{2-} unit in the presence of an applied field with that in $\text{Cu}^0\text{SO}_4^{2-}$ serves to illustrate the ionic nature of the bonding. The lower binding energy of HSO_4^- compared with SO_4^{2-} means, that for an equivalent adsorption orientation, the frequency shifts observed for HSO_4^- may be less than for SO_4^{2-} . However, since the frequency shifts are very dependent on adsorption geometry, this statement cannot be taken as general.

The $\text{Cu}_4^0\text{SO}_4^{2-}$ calculations illustrate that, even accounting for artifacts due to the cluster model, the 3-down multidentate structure of $\text{Cu}_4^0\text{SO}_4^{2-}$ is energetically much more favourable than the 1-down hollow site adsorption for Cu(111). This is mainly due to the very favourable position of the oxygen atoms over the Cu atoms on Cu(111). The comparison of the SO_4^{2-} structure in $\text{Cu}_4^0\text{SO}_4^{2-}$ with the earlier structures indicates that the qualitative nature of the frequency shifts for SO_4^{2-} may be deduced from the geometric distortions of the SO_4^{2-} units. Finally, the structure of the SO_4^{2-} unit in the 1-down $\text{Cu}_4^0\text{SO}_4^{2-}$ cluster indicates the possible formation of a weak chemical bond when compared to the 3-down $\text{Cu}_4^0\text{SO}_4^{2-}$ structure, which is electrostatically bound.

Continuing and future work includes the consideration of more structures for $\text{Cu}^0\text{SO}_4^{2-}$ and $\text{Cu}^0\text{HSO}_4^-$, the computation of harmonic frequencies and IR intensities for these species, the optimization of additional structures for the larger $\text{Cu}_4^0\text{SO}_4^{2-}$ structures and the consideration of even larger clusters such as $\text{Cu}_{10}^0\text{SO}_4^{2-}$. When combined with the current results, these should give more insight into the interaction of SO_4^{2-} and HSO_4^- with metals and metal surfaces.

6 Acknowledgements

This work has been supported in part by the Office of Naval Research. L. A. B. would like to thank J. E. Rice and P. S. Bagus for helpful discussions.

References

- [1] K. Kunimatsu, M. G. Samant, H. Seki, and M. R. Philpott, *J. Electroanal. Chem.* **243**, 203 (1988).
- [2] K. Kunimatsu, M. G. Samant, and H. Seki, *J. Electroanal. Chem.* **258**, 163 (1989).

- [3] M. G. Samant, K. Kunimatsu, H. Seki, and M. R. Philpott, *J. Electroanal. Chem.* **280**, 391 (1990).
- [4] P. W. Faguy, N. Markovic, R. R. Adzic, C. A. Fierro, and E. B. Yeager, *J. Electroanal. Chem.* **289**, 245 (1990).
- [5] L. Blum, H. D. Abruna, J. White, J. G. Gordon II, G. L. Borges, M. G. Samant, and O. R. Melroy, *J. Chem. Phys.* **85**, 6732 (1986).
- [6] O. R. Melroy, M. Samant, G. L. Borges, J. G. Gordon II, L. Blum, J. H. White, M. J. Albarelli, M. McMillan, and H. D. Abruna, *Langmuir* **4**, 728 (1988).
- [7] M. R. Philpott, R. Corn, W. G. Golden, K. Kunimatsu, and H. Seki, *Raman and Infrared Spectroscopy of Molecules Adsorbed on Metal Electrodes*, in *Dynamics on Surfaces*, edited by B. Pullman, J. Jortner, A. Nitzan, and B. Gerber, pp. 401-412, D. Reidel, Holland, 1984, Proceedings of the 11th Jerusalem Symposium on Quantum Chemistry and Biology, April 30-May 3, 1984.
- [8] A. Tadjeddine, D. Guay, M. Ladouceur, and G. Tourillon, *Phys. Rev. Lett.* **66**, 2235 (1991).
- [9] G. Tourillon, D. Guay, and A. Tadjeddine, *J. Electroanal. Chem.* **289**, 263 (1990).
- [10] C. B. Ehlers and J. L. Stickney, *Surf. Sci.* **239**, 85 (1990).
- [11] D. M. Kolb, *Ber. Bunsenges Phys. Chem.* **92**, 1175 (1988).
- [12] P. S. Bagus and F. Illas, *Phys. Rev. C* **47**, 10852 (1990).
- [13] P. S. Bagus, C. J. Nelin, W. Müller, M. R. Philpott, and H. Seki, *Phys. Rev. Lett.* **58**, 559 (1987).
- [14] C. J. Nelin, P. S. Bagus, and M. R. Philpott, *J. Chem. Phys.* **87**, 2170 (1987).
- [15] P. S. Bagus, G. Pacchioni, and M. R. Philpott, *J. Chem. Phys.* **90**, 4287 (1988).
- [16] G. Pacchioni, P. S. Bagus, and M. R. Philpott, *Z. Phys.* **D12**, 543 (1989).
- [17] M. Samant, R. Viswanathan, H. Seki, P. S. Bagus, C. J. Nelin, and M. R. Philpott, *J. Chem. Phys.* **89**, 583 (1988).
- [18] M. Samant, K. Kunimatsu, R. Viswanathan, H. Seki, G. Pacchioni, P. S. Bagus, and M. R. Philpott, *Langmuir* **7**, 1261 (1991).
- [19] L. A. Barnes, B. Liu, and M. R. Philpott, *Model Studies of the Adsorption of Sulfate and Bisulfate on Copper*, to be published (1992).

- [20] F. Anson, *Accounts Chem. Res.* **8**, 400 (1975).
- [21] J. O. Bockris and A. K. N. Reddy, *Modern Electrochemistry*, Plenum Press, New York, 1973.
- [22] G. Valette, *J. Electroanal. Chem.* **122**, 285 (1981).
- [23] R. I. Tucceri and D. Posadas, *J. Electroanal. Chem.* **191**, 387 (1985).
- [24] W. Stoeckel and R. Schumacher, *Ber. Bunsenges Phys. Chem.* **91**, 345 (1987).
- [25] S. Strbac and R. R. Adzic, *J. Electroanal. Chem.* **249**, 291 (1988).
- [26] J. Clavilier, A. Hamelin, and G. Valette, *C. R. Acad. Sci. Paris C265*, 221 (1967).
- [27] P. Zelenay, L. M. Rice-Jackson, and A. Wieckowski, *J. Electroanal. Chem.* **283**, 389 (1990).
- [28] P. Zelenay, L. M. Rice-Jackson, J. Gawlowski, and A. Wieckowski, *Surf. Sci.* **256**, 253 (1991).
- [29] P. Zelenay and A. Wieckowski, *J. Electrochem. Soc.* **139** 2552 (1992).
- [30] O. M. Magnussen, J. Hotlos, R. J. Nichols, D. M. Kolb, and R. J. Behm, *Phys. Rev. Lett.* **64**, 2929 (1990).
- [31] S. Manne, P. K. Hansma, J. Massie, V. B. Elings, and A. A. Gewirth, *Science* **251**, 183 (1991).
- [32] D. B. Parry, M. G. Samant, H. Seki, M. R. Philpott, and K. Ashley, *In Situ FTIR Study of Bisulfate and Sulfate Adsorption on Gold Electrodes, with and without Under Potential Deposition of Copper*, submitted for publication, *Langmuir*, (1992).
- [33] Y. R. Shen, *Principles of Nonlinear Optics*, Wiley, New York, 1984.
- [34] D. J. Campbell and R. M. Corn, *J. Phys. Chem.* **91**, 345 (1987).
- [35] J. M. Robinson and G. L. Richmond, *Electrochim. Acta* **34**, 1639 (1989).
- [36] R. W. G. Wyckoff, *Crystal Structures*, volume 3, Wiley Interscience, New York, second edition, 1965.
- [37] T. H. Dunning, Jr. and P. J. Hay, *Gaussian Basis Sets for Molecular Calculations*, in *Modern Theoretical Chemistry*, edited by H. F. Schaefer, III, volume 3, chapter 1, pp. 1-27, Plenum Press, 1977.

- [38] S. Huzinaga, *J. Chem. Phys.* **42**, 1293 (1965).
- [39] T. H. Dunning, Jr., *J. Chem. Phys.* **53**, 2823 (1970).
- [40] R. Ahlrichs and P. R. Taylor, *J. Chim. Phys.* **78**, 316 (1981).
- [41] A. J. H. Wachters, *J. Chem. Phys.* **52**, 1033 (1970).
- [42] P. J. Hay, *J. Chem. Phys.* **66**, 4377 (1977).
- [43] R. D. Amos and J. E. Rice, 'CADPAC: The Cambridge Analytic Derivatives Package', issue 4.0, Cambridge, 1987.
- [44] C. W. Murray and R. D. Amos, 'The Cambridge Direct SCF Program', Cambridge, 1989.
- [45] M. Duran, J. L. André, A. Lledós, and J. Bertrán, *J. Chem. Phys.* **90**, 328 (1989).
- [46] F. A. Cotton, B. A. Frenz, and D. L. Hunter, *Acta Cryst.* **B31**, 302 (1975).
- [47] R. J. Nelmes, *Acta Cryst.* **B27**, 272 (1971).
- [48] *Handbook of Chemistry*, The Chemical Society of Japan, 11-651 (1984).
- [49] B. S. Dawson, D. E. Irish, and G. E. Toogood, *J. Phys. Chem.* **90**, 334 (1986).
- [50] P. S. Bagus, C. J. Nelin, K. Herman, and M. R. Philpott, *Phys. Rev. Rap. Commun.* **36**, 8169 (1987).